ARL-TR-10363 ● JUNE 2026

Densification of Binder Jet Silicon Carbide Ceramics through Polymer Infiltration and Pyrolysis of Preceramic Polymer

by Emily Vanderploeg, Jaya Penn, Matthew Ivill, Jennifer Bennett, and Nicholas Ku

NOTICES

Disclaimers

The findings in this report are not to be construed as an official Department of the Army position unless so designated by other authorized documents.

Citation of manufacturer's or trade names does not constitute an official endorsement or approval of the use thereof.

Destroy this report when it is no longer needed. Do not return it to the originator.

ARL-TR-10363 ● JUNE 2026

Densification of Binder Jet Silicon Carbide Ceramics through Polymer Infiltration and Pyrolysis of Preceramic Polymer

Matthew Ivill and Nicholas Ku
DEVCOM Army Research Laboratory

Emily Vanderploeg, Jaya Penn, and Jennifer Bennett
U.S. Military Academy

REPORT DOCUMENTATION PAGE

1. REPORT DATE	2. REPORT TYPE	3. DATES COVERED	
		START DATE	END DATE
June 2026	Technical Report	June 3, 2023	April 7, 2026

4. TITLE AND SUBTITLE
Densification of Binder Jet Silicon Carbide Ceramics through Polymer Infiltration and Pyrolysis of Preceramic Polymer

5a. CONTRACT NUMBER	5b. GRANT NUMBER	5c. PROGRAM ELEMENT NUMBER
5d. PROJECT NUMBER	**5e. TASK NUMBER**	**5f. WORK UNIT NUMBER**

6. AUTHOR(S)
Emily Vanderploeg, Jaya Penn, Matthew Ivill, Jennifer Bennett, and Nicholas Ku

7. PERFORMING ORGANIZATION NAME(S) AND ADDRESS(ES)	8. PERFORMING ORGANIZATION REPORT NUMBER
DEVCOM Army Research Laboratory ATTN: FCDD-RLA-ME Aberdeen Proving Ground, MD 21005	ARL-TR-10363

9. SPONSORING/MONITORING AGENCY NAME(S) AND ADDRESS(ES)	10. SPONSOR/MONITOR'S ACRONYM(S)	11. SPONSOR/MONITOR'S REPORT NUMBER(S)

12. DISTRIBUTION/AVAILABILITY STATEMENT
DISTRIBUTION STATEMENT A. Approved for public release: distribution unlimited.

13. SUPPLEMENTARY NOTES
ORCIDs: Emily Vanderploeg, 0009-0004-9109-3499; Jaya Penn, 0009-0000-0785-5915; Matthew Ivill, 0009-0009-4862-4983; Jennifer Bennett, 0000-0001-9193-3583; Nicholas Ku, 0000-0002-1276-4927

14. ABSTRACT
Ceramic materials, known for their high strength and hardness, are increasingly used in structural applications under high strain rates. However, the high hardness and intrinsic brittleness of ceramics limit the ability to machine structural parts with complex and intricate shapes using traditional manufacturing methods. When additive manufacturing techniques are used, particularly binder jetting, it is possible to fabricate geometrically complex ceramic components with materials such as silicon carbide (SiC). This study focuses on polymer infiltration and pyrolysis (PIP) as a net-shape densification process, leveraging a polycarbosilane polymer precursor, Starfire SMP-10, to infiltrate green bodies and densify them without inducing significant shrinkage. The goal is to attain a material density close to theoretical values without resorting to sintering. This study also involves the selection of suitable ceramic powders through powder analysis, considering factors such as flowability and tap density. Results indicate promising increases in density with double infiltration, although leakage of SMP-10 during heat treatments poses challenges. Scanning electron microscope imaging reveals nonuniform infiltration, particularly in the center of samples, potentially affecting densification. Despite these challenges, this study underscores the potential of PIP for densifying ceramic green bodies in binder jetting applications, albeit with the need for refinement in process parameters and precursor selection to mitigate leakage and achieve uniform densification.

15. SUBJECT TERMS
Sciences of Extreme Materials, ceramic processing, silicon carbide, preceramic polymers, polymer infiltration and pyrolysis, polycarbosilane

16. SECURITY CLASSIFICATION OF:			17. LIMITATION OF ABSTRACT	18. NUMBER OF PAGES
a. REPORT	b. ABSTRACT	C. THIS PAGE		
UNCLASSIFIED	UNCLASSIFIED	UNCLASSIFIED	UU	21

19a. NAME OF RESPONSIBLE PERSON	19b. PHONE NUMBER *(Include area code)*
Nicholas Ku	(520) 687-0226

STANDARD FORM 298 (REV. 5/2020)
Prescribed by ANSI Std. Z39.18

Contents

List of Figures

1. Introduction

Ceramic materials are currently used in structural applications at high strain rates due to their high strengths, high hardness, and low density. Silicon carbide (SiC) has high hardness, strength, melting point, and resistance to oxidation while having a relatively low density (3.21 g/mL), which makes it ideal for application in extreme environments.[1] However, traditional manufacturing methods, such as uniaxial hot pressing, greatly limit the geometry of produced parts. Additive manufacturing (AM) enables the forming of ceramics with complex geometries. Advantages for AM of SiC include complex designs, customization, reduced material waste, and elimination of cost- and time-intensive postprocess machining. Another added value is the ability to optimize and rapidly prototype designs.[2]

Binder jetting is an AM process in which an industrial printhead selectively deposits a liquid binding agent onto a thin layer of powder particles to build near-net shape of complex geometry parts. The technique involves repeated layer-by-layer process of adding the ceramic powder and binder fluid in sequence, according to a map from a digital design file, until the object is complete.[3] A major restriction of binder jetting is that the powder feedstock generally needs to be coarse in size to allow the necessary flowability for the additive process.[4] This leads to overall low-bulk density of the formed green bodies that can result in inferior mechanical properties of printed parts, a major limitation of binder jetting.[5]

To achieve the optimal material properties that are desirable in a ceramic, the green body would have to undergo a separate densification process. Traditionally, this densification process would occur through sintering, which causes the green body to shrink from its printed shape and thereby adding a significant challenge in using AM for geometrically complex shapes. In addition, pressureless sintering of SiC requires high-processing temperatures as well as fine starting particle sizes[6] that would be prohibitive for use as a binder jet feedstock powder.[7] Du et al.[8] showed that using a bimodal size distribution in the feedstock can increase the green density of the printed part, but only by a modest 5%. As a result, various alternative methods to densify these green bodies are required, such as chemical vapor infiltration (CVI),[9] liquid metal infiltration and reaction bonding (LMRB),[10–12] and polymer infiltration and pyrolysis (PIP).[13,14]

In each case, technical challenges exist for utilizing each densification method. CVI requires some dimensional limitations because the maximum thickness of the part is limited to the infiltration distance of the chemical vapor. Binder jet parts densified by CVI can often exhibit density gradients, where parts have a dense outer layer but maintain a porous interior.[5] LMRB has incomplete reaction of the liquid

silicon that can have detrimental effects on the property and performance of the SiC material. Even optimized parts can have residual silicon contents of 15%.[11]

PIP processing involves infiltrating the ceramic green body formed by binder jet with a preceramic polymer. The infiltrated body is then cured to stabilize the infilled polymer via crosslinking, followed by a higher-temperature pyrolization step to convert the polymer into an amorphous ceramic matrix. This process involves significant volumetric shrinkage of the polymer phase, where cracks and pores are opened in the matrix of transformed polymer.[15,16] A subsequent infiltration and pyrolysis cycle is then performed to fill in the cracks and pores from the first PIP cycle. These cycles are repeated until the ceramic body is fully densified. Cramer et al.[12] used polycarbosiloxane as a preceramic polymer to densify binder jet SiC parts by a PIP process. Polycarbosiloxane is a precursor for SiOC, so the resultant part was an SiC/SiOC composite.[13] Wang et al.[14] further investigated densification with a polycarbosiloxane polymer and was able to increase part density by performing nine iterative PIP cycles. Both studies showed the feasibility of using a PIP process with preceramic polymers to densify SiC parts formed by binder jet, although any method to reduce the number of iterative PIP cycles would reduce processing time and cost. To densify SiC green bodies with SiC instead of SiOC, the preceramic polymer chemistry needs to be changed to a polycarbosilane. This polymer pyrolyzes with the correct chemistry to produce SiC.[16]

In this study, we investigated various sizes of SiC powder feedstocks to understand their effect on printability and densification by the PIP processing. We used commercial polycarbosilane as a preceramic polymer and investigated preheat treatment to understand its effect on the infiltration, yield of the polymer, and efficiency of the PIP process.

2. Methodology

The SiC powders used in this study were sourced by Panadyne (Montgomeryville, Pennsylvania), and three variants were investigated: 240, 500, and 500 PHD. The preceramic polymer used for the PIP densification process was SMP-10 from Starfire Systems Inc. (Glenville, New York). Per the manufacturer, SMP-10 is a one-component, liquid polycarbosilane precursor, to form near-stoichiometric SiC after thermal treatment.

Particle-sized distributions were measured using a Horiba (Kyoto, Japan) LA-960, and water was used as the dispersant system. The tapped density of the powders was measured using a Quantachrome (Boynton Beach, Florida) Autotap system, and a 10-mL glass-graduated cylinder was used as the test vessel. Scanning electron

microscopy (SEM) was conducted using a Thermo Fisher Scientific (Waltham, Massachusetts) Phenom XL, using the back-scattered detector for imaging. Calorimetry of the polymer was measured using a TA Instruments SDT Q600 DSC-TGA (New Castle, Delaware). All samples were run up to 1500 °C at a heating rate of 10 °C/min under flowing argon using an alumina crucible.

To test precursor infiltration of the feedstock powders, sample green bodies with deliberately low density were created to simulate the light powder-packing and low-density representative of samples typically produced by binder jet manufacturing. The sample geometry was round pucks 25 mm in diameter and 5 mm in height for further testing. To form the samples, 4.5 g of SiC powder along with 5 wt% ExOne Aquafuse binder was placed in a Teflon ring and uniaxially pressed to a pressure of 10 kPa. The sample was then removed and heated to cure the binder at 180 °C for 4 h. The samples were then infiltrated with SMP-10 precursor using a vacuum infiltration method. To infiltrate these samples, a vacuum vessel was equipped with a top drip spout that allowed the precursors to leak into the samples under vacuum. The purpose of conducting the infiltration under vacuum was to remove gas within the samples after the binder cure and ensure the samples became completely saturated with the polymer precursor. The samples were placed under vacuum at −760 mmHg pressure for 30 min. The SMP-10 precursor was then dripped on top of the samples under vacuum until they were completely covered. The samples were then held under vacuum for an additional 30 min to ensure maximum infiltration. Samples were then removed from the vacuum and the precursor, and the excess precursor was allowed to drip off before the samples were immediately pyrolyzed.

For the pyrolysis of the infiltrated samples, the sample was heated at 1 °C/min up to 650 °C, where it was held for 2 h. The temperature was then raised at 3 °C/min up to 850 °C, where it was held for one additional hour. After each of these treatments, the mass, geometric volume, and geometric density of the samples were taken and recorded.

3. Results and Discussion

3.1 Powder Feedstock Characterization

The SiC powder variants were tested for their suitability as feedstocks for the binder jetting process. A powder needs to possess key bulk properties to ensure it is suitable for binder jetting, primarily flowability and packability. To measure both flowability and initial density, particle sizing and tap density were taken initially. Particle sizing is shown in Figure 1 and tap density is shown in Figure 2. The d50

percentile of the particle size distribution for Panadyne 500, 500 PHD, and 240 are 16.01, 12.49, and 60.55 µm, respectively. The Panadyne 500 and 500 PHD powder had very similar particle size and exhibited similar packing behavior under tapping. The PHD variant of the powder did tap to a higher density, which would be advantageous as a feedstock because the green density of a binder jet part would therefore be higher. The Panadyne 240 powder has a significantly larger particle size and size distribution, which led to a higher tap density. The powder also reached its maximum tapped density in fewer taps, which is indicative of a powder with increased packability and flowability.

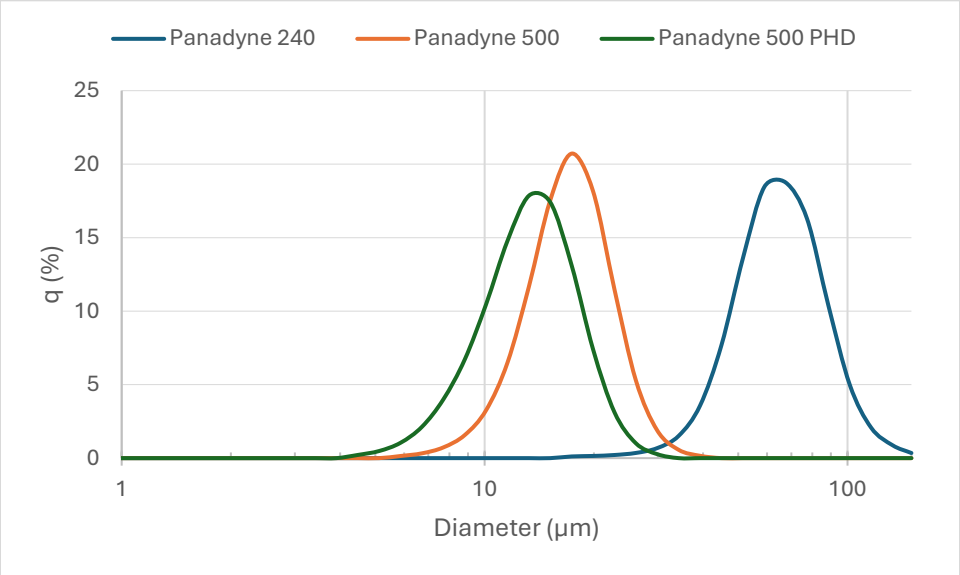

Figure 1. Particle size distributions for Panadyne 240, Panadyne 500, and Panadyne 500 PHD.

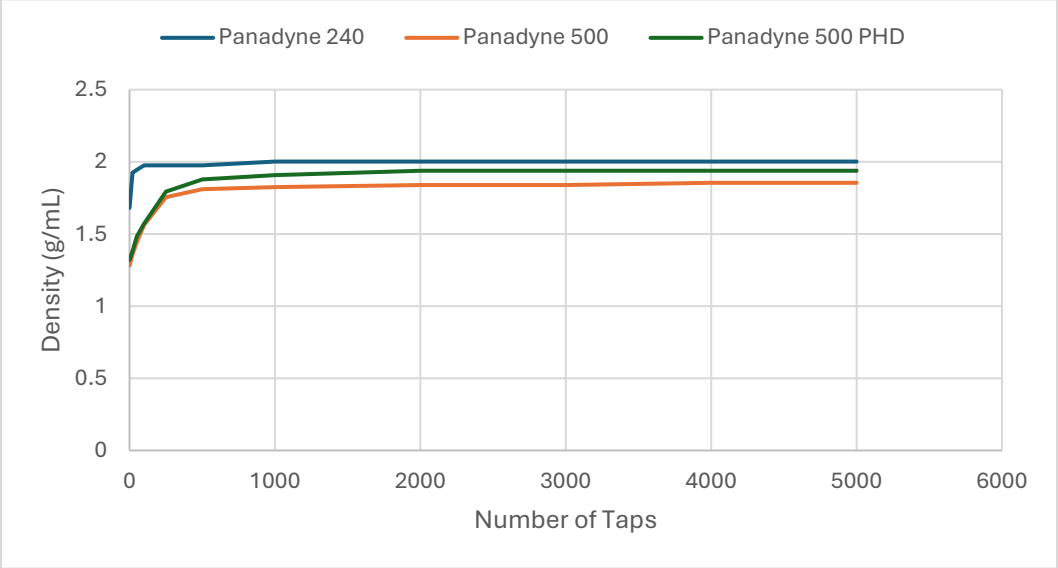

Figure 2. Tap density for various ceramic powders as a function of number of taps.

To see if there were improvements to the tap density from homogeneous sample to a bimodal mix of powder sizing, tap density was also taken for various combinations of Panadyne 240 SiC and Panadyne 500 PHD SiC. Figures 3 and 4 show the optimization of tap density with bimodal distribution. The results show an increase in tapped density with the inclusion of fine Panadyne 500 PHD powder, until a maximum tapped density was achieved at 25 wt% inclusion. Above a composition of 25 wt% fine particles, the tapped density decreased. Therefore, the composition with the maximum tapped density found was 25 wt% Panadyne 500 PHD SiC. When comparing the tapped density behavior of the blended composition to the monomodal powder, the blended powder exhibited a higher tapped density, but it also required more taps to reach its maximum tapped density value. The increased time to reach maximum packing under tapping is indicative of a powder feedstock with a reduced flowability.

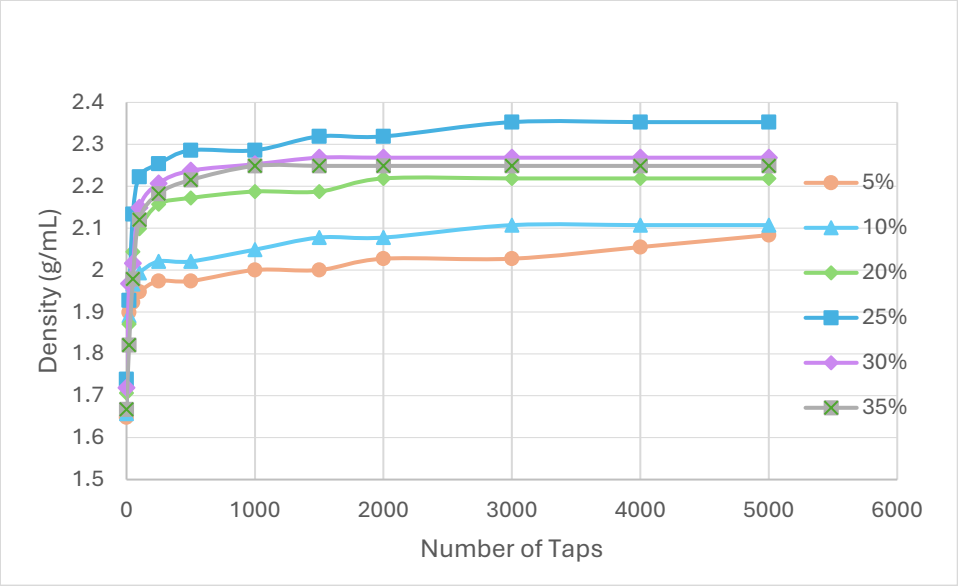

Figure 3. Tap density for bimodal distribution of Panadyne 240 SiC and Panadyne 500 PHD SiC, labeled by wt% fine powder.

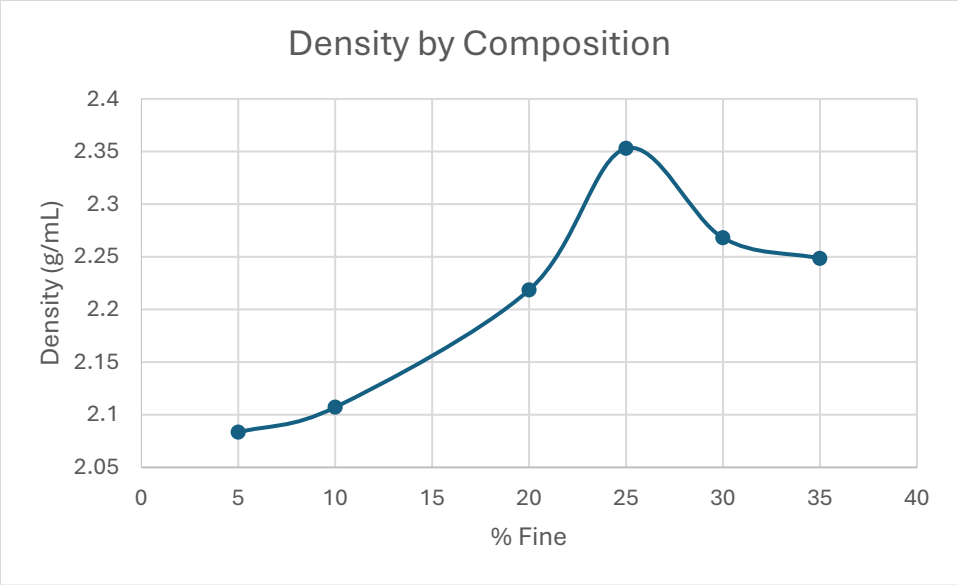

Figure 4. Effect on maximum tapped density by the composition of bimodal distributions of Panadyne 240 SiC and Panadyne 500 PHD SiC, labeled by wt% fine powder.

3.2 Polymer Characterization

The SMP-10 preceramic polymer needs to be pyrolyzed in the PIP densification process. Therefore, the thermal behavior of the polymer was characterized with the differential scanning calorimetry (DSC) data shown in Figure 5. The peaks and inflection points in the graph are indicative of heat flow, showing temperatures that correspond to curing, pyrolization, and crystallization of the pucks. Key peaks identified were 185, 269, 600, 850, 1100, 1290, and 1376 °C. Almost all the mass loss in the polymer occurred below 700 °C, with an inflection point and corresponding peak in heat flow at approximately 185 °C. The maximum weight loss was 30% of the initial weight. The weight of the sample increased after 1150 °C, but this may be due to the reaction of the sample with the alumina crucible during the test as well as potential oxidation of the sample.

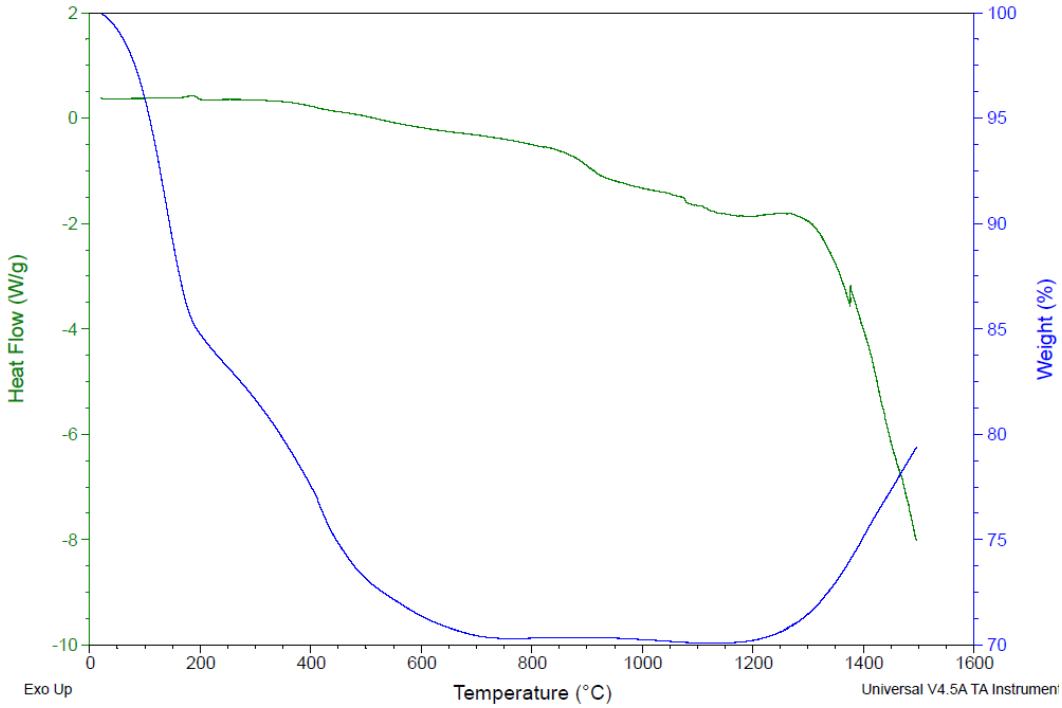

Figure 5. Differential calorimetry data of SMP-10 showing both heat flow and wt% as a function of temperature.

3.3 Polymer Infiltration and Pyrolysis

After two cycles of the PIP process, the overall mass and density increased. Figure 6 shows the mass of the green bodies after infiltration and pyrolysis. Infiltration with the ceramic sample leads to an increase in the mass of the sample; however, it is key to note that there is a subsequent loss in sample mass after each pyrolysis heat treatment, which is expected due to the mass loss of the polymer measured by the DSC. The expectation is that the mass loss during pyrolysis is due to various volatile products being released. These products may include CO, H_2, H_2O, and CO_2 and various hydrocarbons including low-molecular–weight oligomers. However, the average mass loss of infilled polymer is higher than the 30% observed by DSC due to SMP-10 leakage during the pyrolysis heating cycles. This "leakage" is shown in Figure 7, with the polymer creating a "grease stain" on the crucible around the sample after heat treatment to 300 °C.

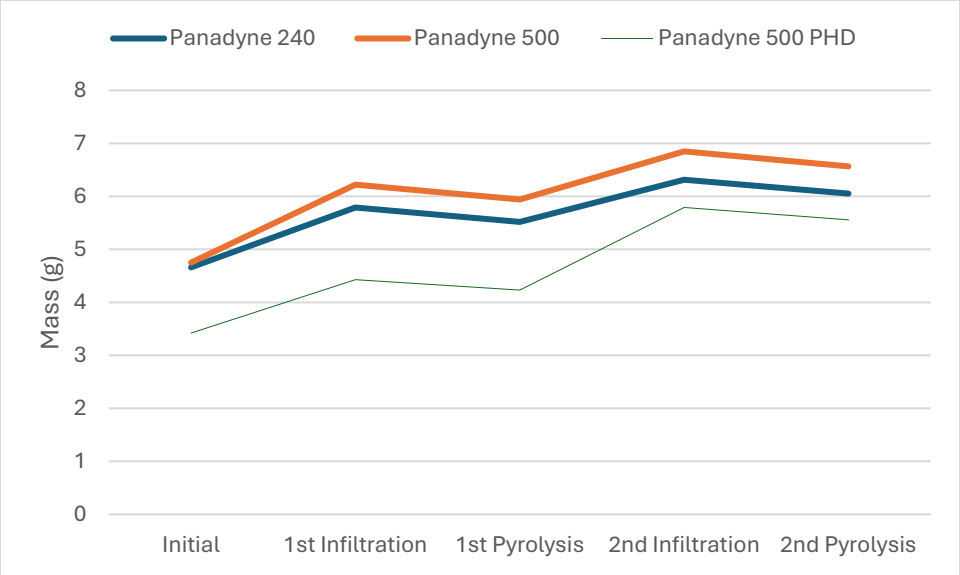

Figure 6. Mass changes in samples through PIP cycles with SMP-10.

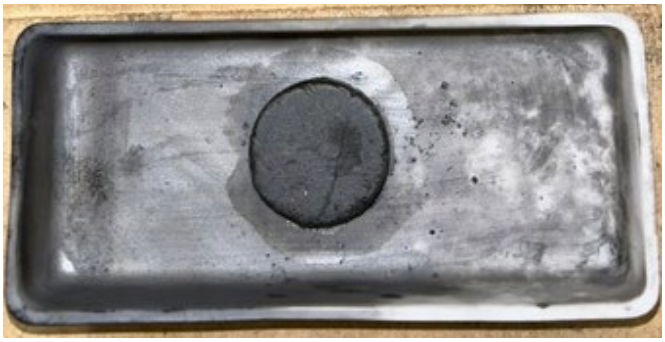

Figure 7. Image of a 1-inch puck of ceramic after infiltration with SMP-10 and heat treatment to 300 °C. Note the ring on the crucible around the base of the puck due to leakage of the polymer out of the puck.

SEM imaging was performed to study the infiltration of the SMP-10 after the infiltrations and heat regimes (Figure 8). The sample puck was cross sectioned, and images were taken near the center and top surface of the sample. During this, the difference in infiltration through the thickness of the samples was apparent. For Panadyne 240, the center section of the sample had more porosity, shown by the black cavities, compared with the less porous top of the same sample (Figure 8). This showed that the distribution of pyrolyzed polymer was inhomogeneous and concentrated on the outer surface of the sample. This may be a result of incomplete infiltration of the polymer, where the material was unable to reach the center of the puck. However, mass comparisons before and after infiltration suggest that approximately 90% of the pore volume were filled by precursor after infiltration. Another likely reason is an increased pore pressure in the ceramic, created by the off gassing of the polymer during the pyrolysis process, with the vapors or volatiles

displacing liquid polymer that is internal to the puck. This displacement would explain the leakage evident in Figure 7.

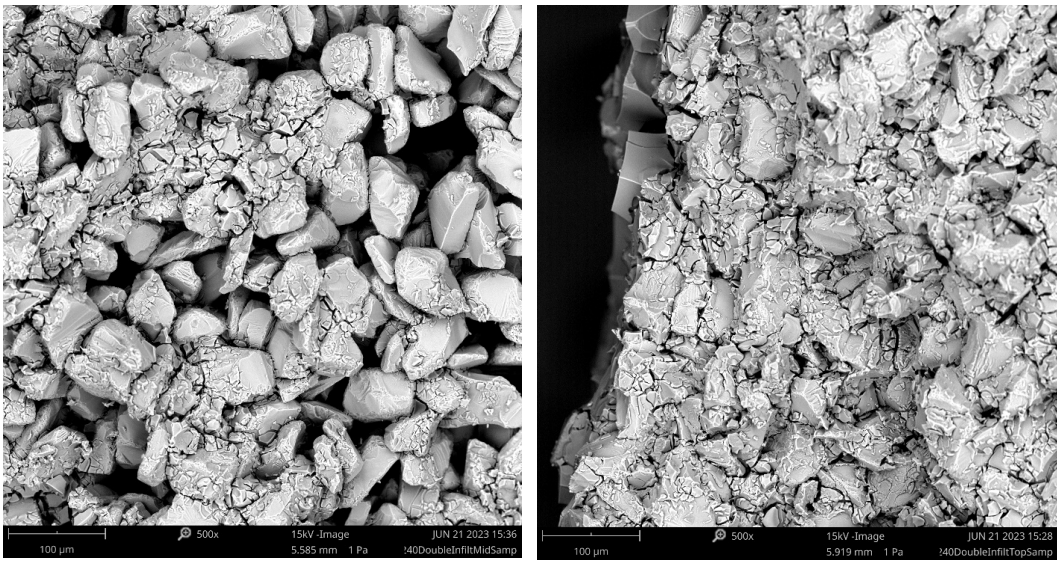

Figure 8. Center (left) and top (right) cross sections of the Panadyne 240 sample after undergoing two infiltrations and pyrolyzing temperatures.

To understand the effect of the leakage during steps of the PIP process, the density of samples was evaluated between the initial green body and a single curing step (without pyrolization) for each powder (Figure 9). A key takeaway from this graph is that the density for Panadyne 240 appears to remain relatively constant. From the mass data in Figure 6, we show that all samples were properly infiltrated with polymer, but the fact that the density of Panadyne 240 sample does not increase significantly suggests that there is loss of material during the curing process. Due to the particle size of the powder, the Panadyne 240 sample has the largest pore size compared with the other samples, allowing the liquid SMP-10 to readily flow from the sample. The heating regime allowed the SMP-10 to heat up and leak out of the sample and, due to the higher porosity of the Panadyne 240, allowed significantly more SMP-10 to leak out. The finer pore size and lower porosity of finer Panadyne powders allowed for more of the polymer to be retained in the sample during curing.

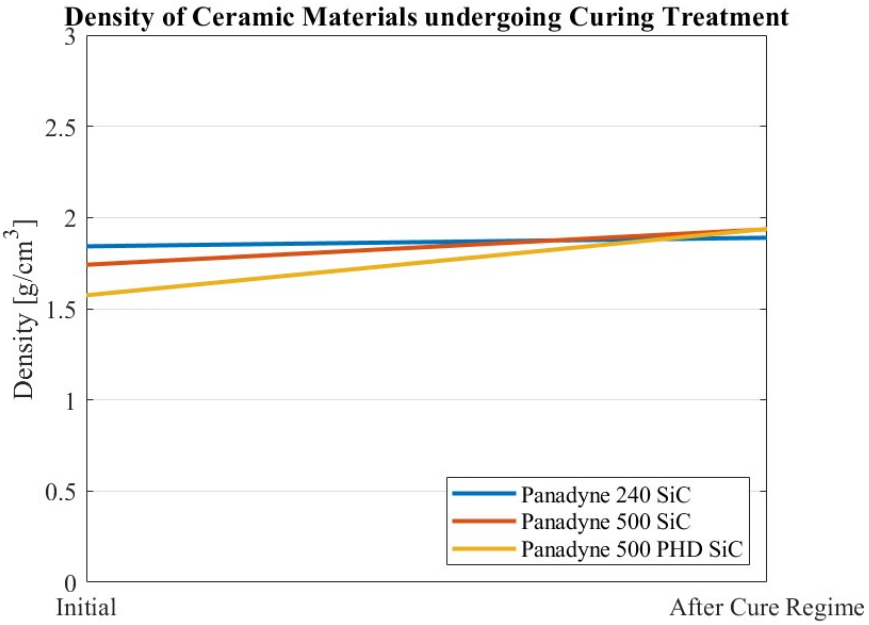

Figure 9. Change in density between the initial green body and after a single curing step.

To track the densification progress of the PIP process, Figure 10 shows the theoretical density (TD) of the part starting with the green body and going through two PIP cycles. For each, the density was measured after pyrolization of the sample and assumes the entire sample consisted of SiC with a density of 3.21 g/mL. This assumption likely underestimates the true density of the sample because the polymer derived ceramic is likely amorphous with low crystallinity and may have a lower density than crystalline SiC. Nevertheless, Figure 10 shows a progressive densification of the sample over two PIP cycles. The largest increase was experienced by the Panadyne 500 PHD sample, which had an increase of 17% TD. This sample also had the lowest green density, suggesting that it had the largest porosity volume of the three samples, which may explain why it was so readily densified though infiltration. If the results were extrapolated, it would require six PIP cycles to reach full density, assuming the increase in density was linear for each successive PIP cycle. This assumption likely would not hold true, because the pore size distribution of the sample would decrease with each PIP cycle, making it more difficult to densify with each successive cycle. More PIP cycles need to be conducted to understand that behavior, although the reported data suggests that understanding feedstock powder size distribution and initial packing could be used to engineer green bodies for more efficient PIP processing.

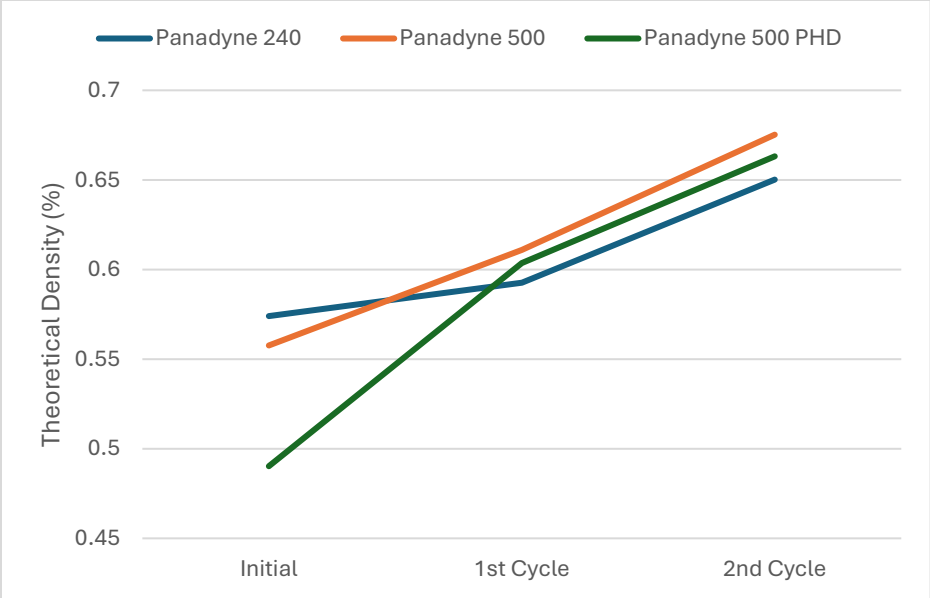

Figure 10. Change in TD of the SiC part over two PIP cycles.

4. Conclusion

Optimizing alternative methods to traditional sintering for the densification of additively manufactured, near-net shape ceramics is an important processing concern for maintaining adequate mechanical performance of the ceramic. This is especially true for parts produced by binder jet manufacturing where the powder particle size and resulting green densities are inherently limited by the binder jet process. PIP processing using polycarbosilane-derived precursors has been used for increasing the bulk density of ceramic matrix composites and likewise provides an attractive method for infiltration and densification of SiC into porous binder jet-manufactured parts. In this report, several powder feedstocks were investigated for applicability to binder jet manufacturing and screened for flowability and packing density. The powders were compacted into low-density green bodies to investigate the performance of SMP-10 liquid infiltration and subsequent densification using sequential PIP processing. Vacuum infiltration of as-received SMP-10 was able to backfill almost 90% of the residual porosity in SiC samples with initial green densities of ranging from 49% to 57% TD. However, subsequent out-gassing of volatile products increases pore pressure and expels liquid polymer during heating before the polymer can fully cure inside the ceramic. This leads to less retained polymer and decreased mass yield. These initial results provide a baseline for optimizing preheat treatment times and thermal cure cycles focused on improving the infiltration and densification of SiC green bodies.

5. References

1. Harris GL, editor. Properties of silicon carbide. Iet; 1995. (emis. Data Review Series; no. 13).
2. Boretti A, Castelletto S. A perspective on 3D printing of silicon carbide. J Eur Ceram Soc. 2024;44(3):1351–1360.
3. Sachs E, Cima M, Cornie J. Three-dimensional printing: rapid tooling and prototypes directly from a CAD model. CIRP Ann. 1990;39(1):201–204.
4. Lv X, Ye F, Cheng L, Fan S, Liu Y. Binder jetting of ceramics: powders, binders, printing parameters, equipment, and post-treatment. Ceram Int. 2019;45(10):12609–12624.
5. Pelz JS, Ku N, Meyers MA, Vargas-Gonzalez LR. Additive manufacturing of structural ceramics: a historical perspective. J Mater Res Technol. 2021;15:670–695.
6. Vargas-Gonzalez LR. Microstructural optimization of solid-state sintered silicon carbide [dissertation]. Georgia Institute of Technology (US); 2010.
7. Bose S et al. 3D printing of ceramics: advantages, challenges, applications, and perspectives. J Am Ceram Soc. 2024;107(12):7879–7920.
8. Du W, Singh M, Singh D. Binder jetting additive manufacturing of silicon carbide ceramics: development of bimodal powder feedstocks by modeling and experimental methods. Ceram Int. 2020;46(12):19701–19707.
9. Koyanagi T, Terrani K, Harrison S, Liu J, Katoh Y. Additive manufacturing of silicon carbide for nuclear applications. J Nucl Mater. 2021;543:152577.
10. Karandikar P, Watkins M, McCormick A, Givens B, Aghajanian M. Additive manufacturing (3D printing) of ceramics: microstructure, properties, and product examples. Proceedings of the 41st International Conference on Advanced Ceramics and Composites: Ceramic Engineering and Science Proceedings. John Wiley & Sons, Inc; 2018;38(3)175–187.
11. Fleisher A et al. Reaction bonding of silicon carbides by binder jet 3D-printing, phenolic resin binder impregnation and capillary liquid silicon infiltration. Ceram Int. 2019;45(14):18023–18029.
12. Cramer CL et al. Properties of SiC-Si made via binder jet 3D printing of SiC powder, carbon addition, and silicon melt infiltration. J Am Ceram Soc. 2021;104(11):5467–5478.

13. Cramer CL et al. Processing and properties of SiC composites made via binder jet 3D printing and infiltration and pyrolysis of preceramic polymer. Int J Ceram Eng Sci. 2020;2(6):320–331.

14. Wang Y, Hou Y, Zhang L, Song Z, Wen G. Silicon carbide ceramics formed by binder jetting: a study focusing on the printing layer thickness and the PIP densification process. Ceram Int. 2024;50(17):30894–30905.

15. Greil P. Polymer derived engineering ceramics. Adv Eng Mater. 2000;2(6):339–348.

16. Colombo P, Mera G, Riedel R, Soraru GD. Polymer-derived ceramics: 40 years of research and innovation in advanced ceramics. J Am Ceram Soc. 2010;93(7):1805–1837.

List of Symbols, Abbreviations, and Acronyms

AM	Additive Manufacturing
CVI	Chemical Vapor Infiltration
DSC	Differential Scanning Calorimetry
LMRB	Liquid Metal Infiltration and Reaction Bonding
PIP	Polymer Infiltration and Pyrolysis
SEM	Scanning Electron Microscopy
SiC	Silicon Carbide
TD	Theoretical Density

1 (PDF)	DEFENSE TECHNICAL INFORMATION CTR DTIC OCA
1 (PDF)	DEVCOM ARL FCDD RLB CB TECH LIB